Domain-Boundary Structure of Styrene–Isoprene Block Copolymer Films Cast from Solution. 4. Molecular-Weight Dependence of Lamellar Microdomains

Takeji Hashimoto,* Mitsuhiro Shibayama, and Hiromichi Kawai

Department of Polymer Chemistry, Faculty of Engineering, Kyoto University, Kyoto 606, Japan. *Received January 30, 1980*

ABSTRACT: A series of diblock polymers of polystyrene and polyisoprene having about equal block molecular weights but different total molecular weights were synthesized to study a relationship between the molecular dimension and the domain size and the thickness of the domain-boundary interphase for the lamellar microdomains in the solid state. Quantitative analyses with the small-angle X-ray scattering technique indicated that the domain identity period varies with the total molecular weight to the $^2/_3$ power, while the interfacial thickness is almost independent of the molecular weight covered in this work. The experimental results were shown to be consistent with the theoretical results based upon random-flight chain statistics in the confined domain space.

I. Introduction

Block polymers composed of incompatible block segments generally form a microdomain structure in the solid state as a consequence of microphase separation of the constituent block chains in the solidification process.[1,2] The microdomain structure in the solid state, including diffuseness of the phase boundaries due to the mixing of the incompatible chains at the interfaces, depends on the molecular weights of the constituent block chains, the thermodynamic interaction parameter, and the temperature (all of which are responsible for equilibrium aspects of the domain morphology) as well as the solidification conditions (factors responsible for nonequilibrium aspects).

The equilibrium aspects of domain morphology involve two requirements: incompressibility and incompatibility. Since the A and B polymers are highly incompatible, A(B)-block chains must be confined to the A(B) domain. There are regions in the domain space which are occupied by pure A- or B-block chains, i.e., the regions having $\tilde{\rho}_A = 1$ or $\tilde{\rho}_B = 1$ as shown in Figure 1. The quantity $\tilde{\rho}_K$ is the relative segment density of the K chain as defined by the ratio of the segment density of the K phase (ρ_K) to that of the bulk pure K polymer (ρ_{0K}). The high degree of incompressibility demands uniform overall segment density everywhere in the domain space.

The morphology of the domain structure, such as equilibrium size, shape, and interfacial thickness, has been described in terms of a balance of three physical factors.[3-8] (i) The repulsive interaction between the A- and B-block segments tends to cause the domain to grow in terms of thicknesses T_A and T_B (Figure 1) so as to reduce the surface-to-volume ratio. Factor i tends to be counterbalanced by two forces of entropic origin: (ii) the loss of conformational entropy to maintain the uniform segment density and (iii) the loss of placement entropy to confine the A–B chemical junctions somewhere in the interfacial region. The three physical factors depend on the molecular weights of the constituent block segments, the interaction parameter, and temperature.

In this series of papers, we explore quantitatively the microdomain structure and the structure of the domain-boundary interphase by the small-angle X-ray scattering (SAXS) technique. Part 1[9] of this series dealt with a paracrystalline analysis of lamellar microdomains for particular block polymers of styrene–isoprene. The main conclusions drawn therefrom are as follows: (i) the lamellae having colloidal dimensions are highly oriented with their boundaries parallel to the bulk film surfaces prepared by the solvent-casting method; (ii) the domain sizes are highly uniform and their spatial arrangement is very regular; (iii) the interfacial thickness is finite.

The domain-boundary structure was more quantitatively evaluated for the lamellar microdomain based upon an analysis of the systematic deviation of the SAXS curve from Porod's law at large scattering angles (part 2).[10] The estimated size of the interfacial thickness and the microdomain size were shown to agree with values predicted from equilibrium theories[4,7] based on the statistical mechanics of random-flight chains in the confined space.

In this paper we further study the domain size and the interfacial thickness as a function of molecular weight for a series of block polymers having lamellar microdomains and quantitatively compare the results with those predicted from equilibrium theories. Moreover, we improve the method for estimating the interfacial thickness t in such a way that the new method is free from the narrow-interphase approximation (see section IV-2). We also change the definition of the interfacial thickness so that it is more appropriate than that previously given. In our previous analyses[10] we have assumed that (i) the A and B segments are symmetric, having identical degrees of polymerization, densities, and statistical segment lengths for the A- and B-block chains, (ii) the statistical segment length of polyisoprene having high 1,2 and 3,4 additions is nearly equal to that of *cis*-1,4-polyisoprene, and (iii) in some cases (based upon the theory of Helfand) the energetic interactions between the A and B segments are localized; thus Debye's interaction-range parameter[11] is assumed to be zero. All of these assumptions have been eliminated in this paper (see section V).

II. Experimental Section

1. Test Specimens. A series of styrene and isoprene diblock copolymers were synthesized by the anionic polymerization technique, using *sec*-BuLi as the initiator and tetrahydrofuran as the polymerization solvent. Samples L-1 to L-3 and sample L-6 were prepared by sequentially polymerizing styrene monomers and then isoprene monomers. On the other hand, samples L-4 and L-5 were prepared by first polymerizing 50 wt % of all styrene monomers and then simultaneously copolymerizing the remaining 50 wt % styrene and isoprene monomers in the reactor.

Table I shows the number-average total molecular weight measured by a high-speed membrane osmometer (in toluene at 37 °C), the weight fraction of polystyrene determined from elemental analysis, the heterogeneity index $\bar{M}_w/\bar{M}_n$ determined from GPC, and the domain identity period as measured by electron microscopy.

The microstructure of polyisoprene prepared by anionic polymerization in tetrahydrofuran was examined by infrared spectroscopy and was estimated to contain 38, 59, and 3% 1,2,

0024-9297/80/2213-1237$01.00/0

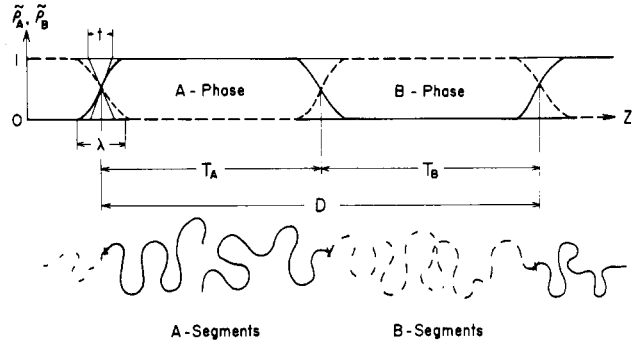

Figure 1. Relative segment density profiles $\tilde{\rho}_A$ and $\tilde{\rho}_B$ of the A and B segments of A–B diblock polymers. Thickness T_A of the A domain and T_B of the B domain, the domain identity period D, and the interfacial thickness of λ and t are defined. The thickness t corresponds to the thickness of the interphase having a linear density gradient as defined by eq 18 in the text.

Table I
Characterization of the Styrene and Isoprene Diblock Polymers

specimen code	$10^{-3}\bar{M}_n$[a]	wt % of PS block[b]	$\bar{M}_w/\bar{M}_n$[c]	D_{EM}, nm
L-1	21	53	1.16	17
L-2	31	40	1.13	24
L-3	49	45	1.13	28
L-4[d]	55	46	1.18	34
L-5[d]	97	51	1.18	46
L-6	102	61	1.18	51

[a] Total molecular weight measured by a high-speed membrane osmometer in toluene at 37 °C. [b] Determined from elemental analysis. [c] Determined from GPC data. [d] Polymerized by a slightly different procedure from the others.

3,4, and 1,4 additions. The detailed procedure has been described elsewhere.[12]

The statistical segment length of the polyisoprene sample having a high vinyl content was also estimated by measuring intrinsic viscosity in a Θ solvent, $K_{PI} \equiv [\langle R^2_{PI}\rangle_0/\bar{M}_n]^{1/2} = 0.072$ nm, or $b_{PI} \equiv [\langle R^2_{PI}\rangle_0/\bar{Z}_n]^{1/2} = 0.59$ nm at the Θ temperature 57.1 °C (in ethyl acetate solution), where $\langle R^2_{PI}\rangle_0$ is the unperturbed chain dimension of polyisoprene and $\bar{M}_n$ and $\bar{Z}_n$ are the number-average molecular weight and degree of polymerization. The detailed procedure is described elsewhere.[12] It should be noted that K_{PI} and b_{PI} are significantly smaller than the corresponding values of 0.081 and 0.67 nm for *cis*-1,4-polyisoprene.[13]

The densities of the pure polymers were measured by the density gradient tube method, and values of 1.05 and 0.925 g/cm^3 for polystyrene and polyisoprene, respectively, were obtained.

The film specimens used for the SAXS experiments and electron microscopic studies were prepared by casting 5% toluene solutions onto a glass plate and evaporating the solvent very gradually at 30 °C for a few days. The film specimens thus formed were further dried under vacuum (10^{-6} torr) for several days until the specimens showed a constant weight.

2. SAXS Measurements. The SAXS intensity distribution was measured with a rotating-anode X-ray generator (Rigaku-Denki Rotaflex RU-Z, operated at 40 kV and 200 mA). The intensity was measured on a conventional low-angle X-ray goniometer (no. 2202, Rigaku-Denki) with a four-slit system and Soller slits between the third and fourth slits. Details of the collimating system, such as the focal spot size, size of the slits, and distances between the slits, as well as the slit-length and -width weighting functions are described elsewhere and will not be repeated here.[14] The intensity was measured with Ni-filtered Cu Kα radiation and a pulse-height analyzer (λ = 0.154 nm). For measurements of the intensity at large scattering angles the widths of the third and fourth slits were enlarged to 0.3 mm so as to gain enough counts of the scattered photons without distortion of the scattering profile. The measured intensity was corrected for air scattering and absorption.

In order to investigate the degree of orientation of the lamellar microdomains with respect to the film normals, the SAXS patterns were also taken with a point-focusing camera (no. 1555, Rigaku-Denki, equivalent to a Huxley-Holmes camera) composed of a bent mirror as a horizontal reflector and a bent quartz monochromator as a vertical reflector.

III. Results

1. Electron Microscopic Studies. In order to study the morphology of the phase-separated microdomain structure, the film specimens were stained by osmium tetraoxide aqueous solution, subsequently cut into a ribbon shape, embedded in epoxy resin, trimmed, and stained again. The restained specimens were ultramicrotomed into thicknesses of about 30 nm for observation under a transmission electron microscope.

Figure 2 shows the transmission electron micrographs. The dark phases correspond to the polyisoprene microdomains selectively stained by osmium tetraoxide while the bright phases are the unstained polystyrene microdomains. All specimens show clearly the alternating lamellar microdomains of polystyrene and polyisoprene, the spacing of which is shown to be uniform and to increase with increasing molecular weight, as shown in Table I.

The relative fraction of the dark and bright phases roughly coincides with the volume fraction of polyisoprene and polystyrene phases. More quantitatively, the fraction could be determined by the paracrystalline analysis as discussed in part II. It is also important to note that although there exists surface waviness in the interfaces, this wavelength seems to be much larger than the estimated interfacial thickness of about 2 nm (see discussion in section IV-2).

2. SAXS. (a) Orientation of Microdomains. The SAXS patterns were taken with the incident beam parallel or normal to the film surfaces. All of the patterns for the L-1 to L-6 specimens exhibited uniaxial orientation of the lamellar normal, the direction perpendicular to the interfaces between the two lamellae, with respect to the direction perpendicular to the film surfaces (film normal) (see Figure 3 for definition).

Figure 4 shows the SAXS patterns for the L-1 to L-6 specimens in which only the first-order scattering maximum is shown for L-1, L-2, L-4, and L-5 and only the scattering maxima up to the third-order are shown for L-3 and L-6. For the L-3 specimen, the first-order maximum is degenerated to zeroth-order diffuse scattering due to an overexposure, and the second-order maximum is so weak that it cannot be observed in the pattern. The third-order maximum is clearly visible in the figure. For the L-6 specimen, the first-order maximum is again degenerated to the zeroth-order scattering. However, in contrast to L-3, the second-order maximum is very strong and the third-order maximum is weakly observed in the patterns. Each pattern shows, however, a number of higher order scattering maxima as typically shown in Figure 5 for L-5 and L-6 or as quantitatively shown in Figure 6.

All of the patterns in Figure 4 appear perpendicular to the film surfaces, indicating that the lamellar normals are highly oriented parallel to the film normals. Although the orientation distributions of the lamellae are not yet analyzed for these polymers, we have previously analyzed the orientation for the S–I diblock polymer (designated as SI-L),[10] which has a molecular weight, chemical composition, and, therefore, SAXS pattern quite similar to that of the L-6 specimen. The SAXS pattern for the SI-L specimen was shown in Figure 2 of ref 10. The azimuthal-angle dependence of the integrated intensity of the pattern (see Figure 3 of ref 10) indicated that the sec-

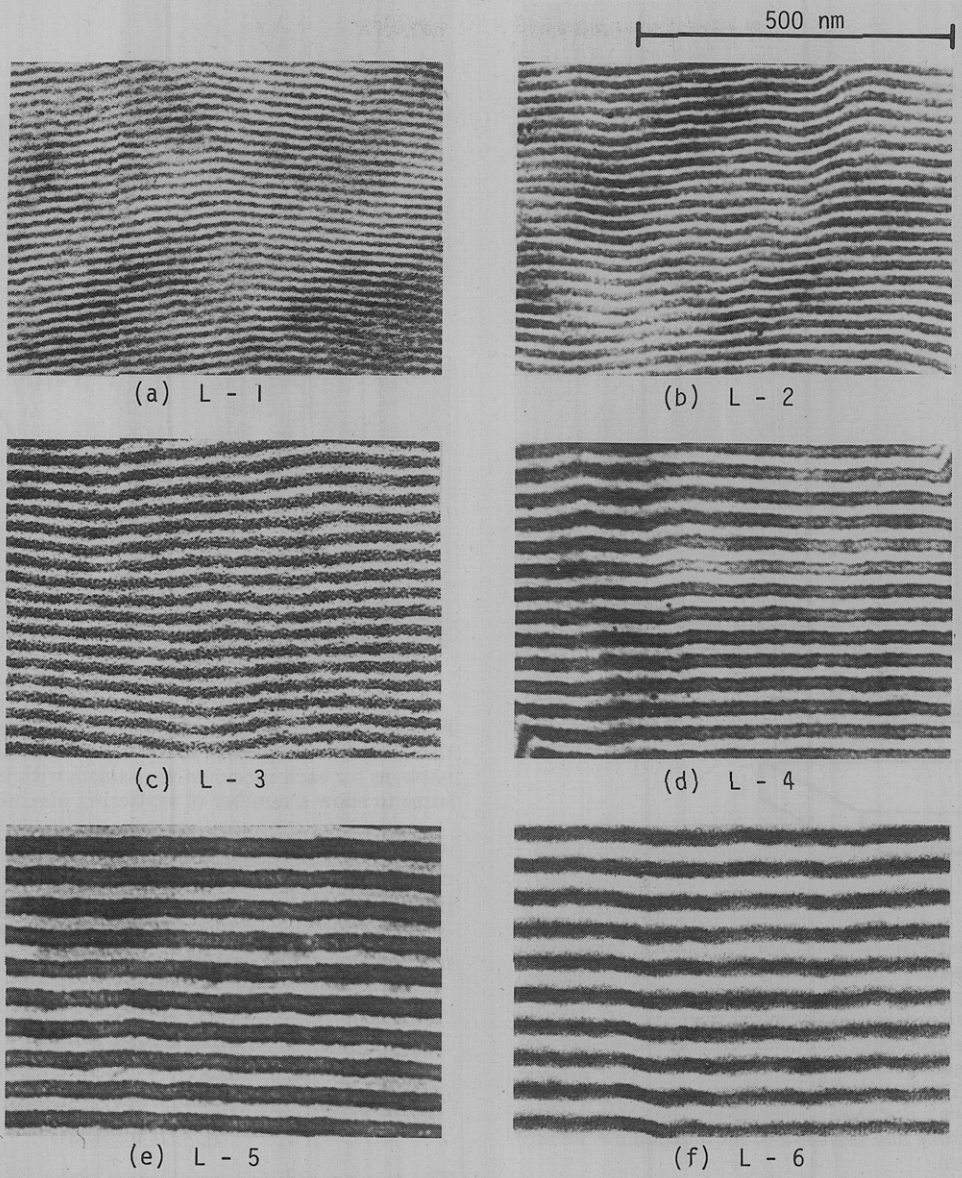

Figure 2. Transmission electron micrographs of the ultrathin sections of the specimens stained by OsO_4.

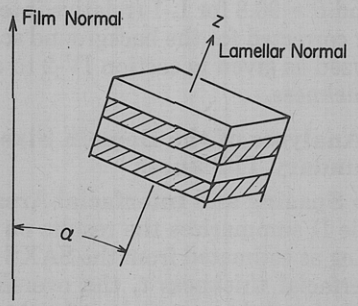

Figure 3. Diagram showing uniaxial orientation of the lamellar normal with respect to the film normal. The angle α is a polar angle specifying the orientation of the lamella.

ond-order orientation factor of the lamellar normal with respect to the film normal, $f_z = [3\langle\cos^2\alpha\rangle - 1]/2$, was 0.95 ($\alpha$ is the angle between the lamellar normal and the film normal as shown in Figure 3). Specimens L-1 to L-6 also seem to have approximately the same degree of lamellar orientation.

This high degree of domain orientation was also observed by Keller, Folkes, and co-workers[15,16] for extruded polystyrene–polybutadiene–polystyrene triblock copolymers. It was also noted in this case that the interfaces are oriented parallel to the surface of the extruded materials. The origin of such a domain-orientation mechanism needs further work.

(b) SAXS Intensity Profiles (Small Angles). The SAXS intensity distributions along the film normal were measured with the line-collimating system as described in section II-2, the specimens being so arranged that the film surface and, therefore, the interface between the domains are set parallel to the line source of the X-ray beam. In this arrangement the scattered intensity distributions should not be affected by the effect of slit-height smearing. The correction for that effect was therefore not performed in subsequent analyses.

Figure 6 shows the SAXS intensity distributions for the series of lamellar microdomains. Each curve shows a number of higher order scattering maxima arising from a single lamellar spacing. The average spacing $\bar{D}$ calculated from each maximum on the basis of Bragg's equation (eq 1) agrees with an error of less than 1.5%. The $\bar{D}$ spacing

$$2\bar{D}\sin\theta = n\lambda \qquad (1)$$

as measured by SAXS agrees quite well with those measured by electron microscopy. The scattering profile may be described in terms of the paracrystalline model as discussed in a previous paper.[9] For example, relative peak

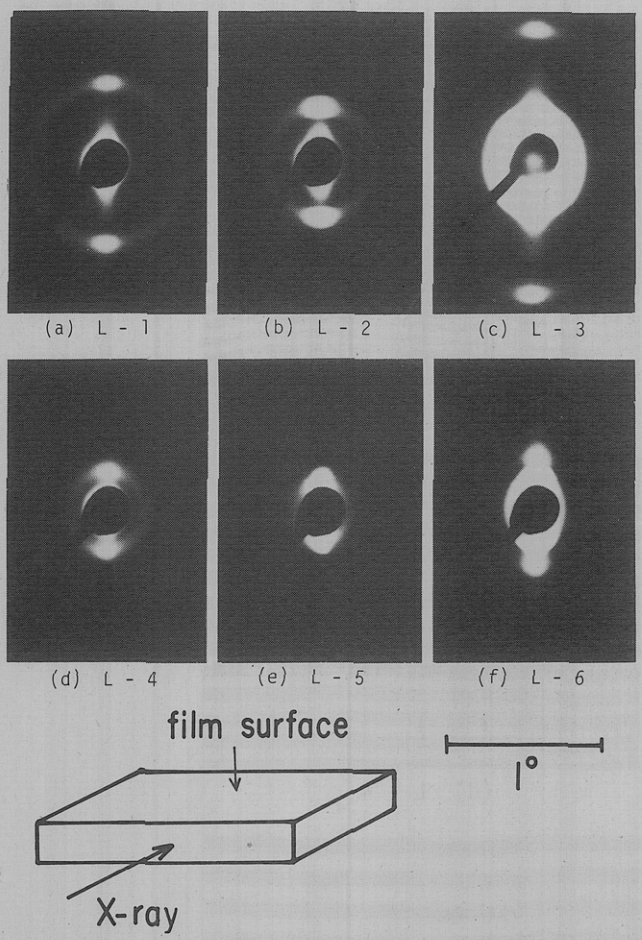

Figure 4. SAXS patterns for specimens L-1 to L-6 taken with the incident beam parallel to the film surfaces. Only the first-order scattering maximum is shown except for specimens L-3 and L-6 for which the first-order maximum is degenerated to the zeroth-order diffuse scattering due to an overexposure. For the L-3 specimen, the second-order maximum is so weak that it is difficult to distinguish but the third-order maximum is clearly visible in the pattern. For the L-6 specimen, the second-order maximum is very strong and the third-order maximum is weakly visible in the pattern.

heights of the higher order scattering maxima primarily depend on the volume fraction of polystyrene or polyisoprene microdomains, and the number of scattering maxima depends upon the uniformity of the domain spacing.

If the spatial arrangement of the domains has a disorder characteristic of paracrystalline statistics, one can estimate the paracrystalline g factor ($g = \Delta D/\bar{D}$, where ΔD is the standard deviation of the identity period D from average $\bar{D}$).[17b] The integral width of the lattice factor for the nth-order maximum $\delta\beta(n)$ is given by

$$\delta\beta(n) = \{1 - \exp(-2\pi^2 n^2 g^2)\}/(2\bar{D}) \simeq \pi^2(gn)^2/\bar{D} \quad (2)$$

The nth-order peak is distinguishable from the background if

$$gn \lesssim 0.35 \quad (3)$$

Thus the fact that the SAXS profile for L-6 exhibits at least up to a ninth-order maximum indicates that $0.035 \lesssim g \lesssim 0.039$;[41] i.e., the paracrystalline distortion is of the order of a few percent. Thus microdomain structure turns out to be very regular and the lamellar thickness is quite uniform.

(c) SAXS Intensity Profile (Tail Region). Figure 7 shows a typical scattering intensity profile (for L-6) at large scattering angles in the SAXS. The intensity increases

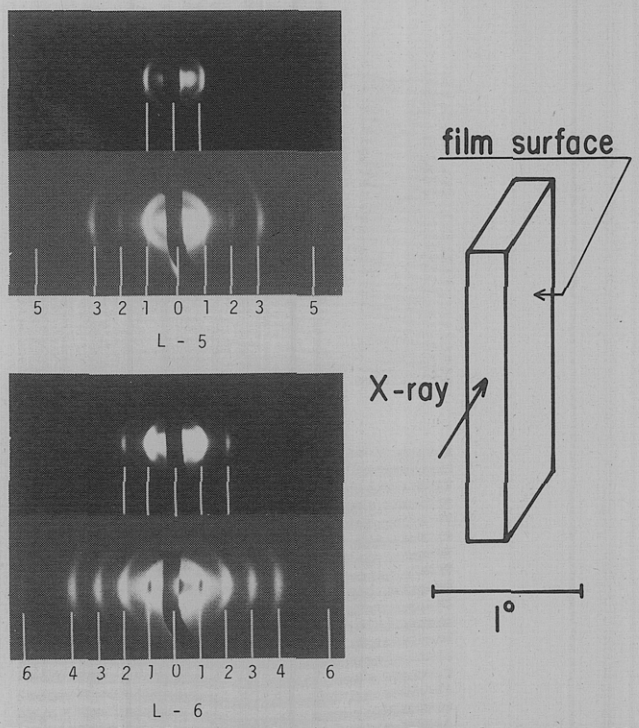

Figure 5. SAXS patterns for specimens L-5 and L-6 taken with the incident beam parallel to the film surface as in the figure. The patterns for each specimen were taken with two different exposures to show a number of scattering maxima.

with increasing scattering angles 2θ due to an increasing contribution from the amorphous scattering within each phase. This background scattering intensity was subtracted from the measured intensity according to empirical procedures proposed by Vonk[18]

$$I_b = as^n + b \quad (4)$$

$$s = (2 \sin \theta)/\lambda$$

or by Ruland[17a]

$$I_b = \alpha \exp(\beta s^2) \quad (5)$$

The two procedures gave almost identical results; e.g., from eq 4, $a = 5.78 \times 10^3$, $n = 2.26$, and $b = 26.0$ and from eq 5, $\alpha = 25.8$ and $\beta = 90.8$ for L-1 (relative intensity scale). The intensity corrected for the background scattering was further analyzed as given in section IV-2 to evaluate the interfacial thickness.

IV. SAXS Analyses of the Domain Size and Domain-Boundary Thickness

1. Domain Spacing and Interfacial Area per Block Chain. Table II summarizes the results on the average domain spacing as estimated from the SAXS ($\bar{D}_{SAXS}$) and lists the interfacial thickness t, the overall interfacial volume fraction f, and the average interfacial area occupied by a block polymer chain S/N.

Figure 8 shows the average domain spacing $\bar{D}$ and the interfacial thickness t as a function of the total molecular weight of the block polymers. It is obvious that the spacing systematically increases with total molecular weight. The straight line in Figure 8 has a slope of $^2/_3$ and gives an empirical relationship

$$\bar{D} = 0.024\bar{M}_n^{2/3} \quad \text{(nm)} \quad (6)$$

The power $^2/_3$ is substantially greater than the power $^1/_2$ expected for the molecular-weight dependence of the unperturbed chain dimensions. This is a consequence that the chain in the domain space expands due to the con-

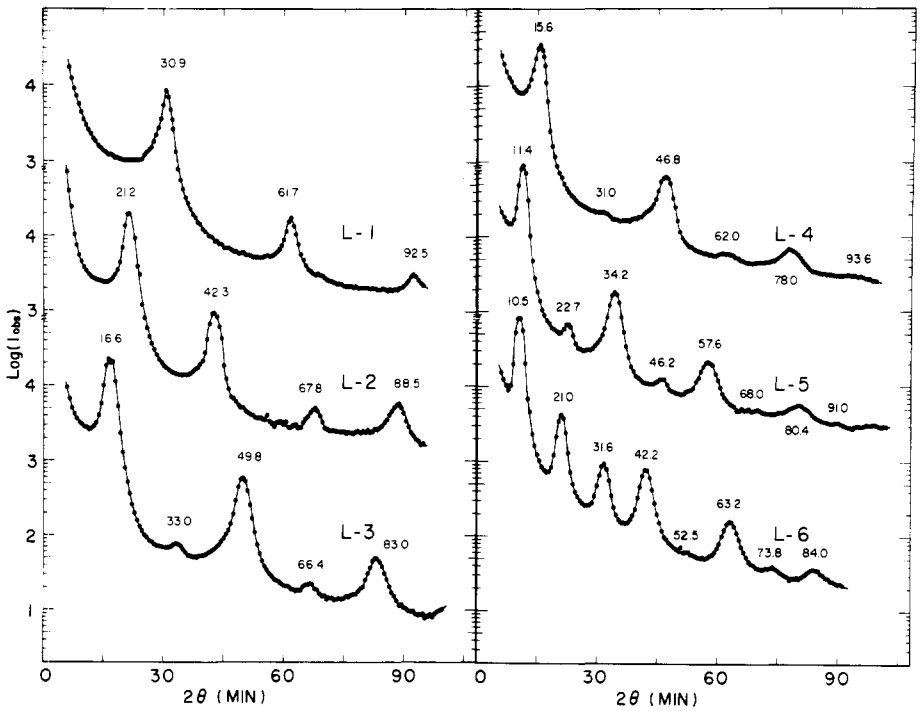

Figure 6. SAXS intensity distributions for a series of lamellar microdomains from specimens L-1 to L-6.

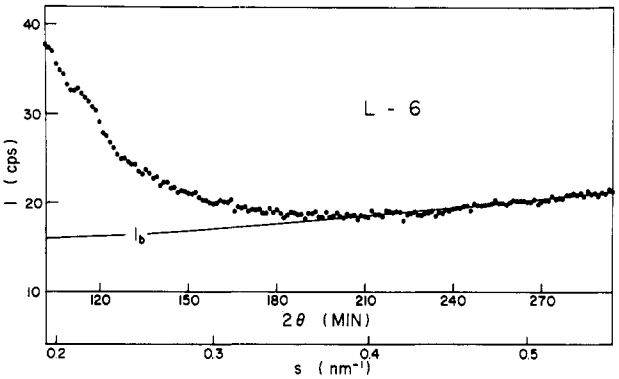

Figure 7. Typical large-angle tail SAXS intensity distribution and the background scattering I_b due to amorphous scattering within each phase.

Table II
Measured Domain Properties of Polystyrene-Polyisoprene Diblock Polymers Having Lamellar Morphology

specimen code	$10^{-3}\bar{M}_n$	wt % PS	domain properties: $\bar{D}_{SAXS}$, nm	t, nm	f	S/N, nm²
L-1	21	53	17.2	2.0 ± 0.2	0.23	4.1
L-2	31	40	24.3	1.7 ± 0.2	0.14	4.2
L-3	49	45	31.9	1.9 ± 0.2	0.19	5.2
L-4[a]	55	46	34.0	2.3 ± 0.2	0.14	5.4
L-5[a]	97	51	46.3	2.6 ± 0.2	0.11	7.1
L-6	102	61	50.3	1.7 ± 0.2	0.067	6.8

[a] Polymerized by a slightly different procedure from the others.

straint volume effect (A(B) chains are restricted to A(B) domains) and to the chain perturbations required to maintain a uniform segment density. This chain expansion depends on molecular weight, thus resulting in a power greater than $^1/_2$.

It should be noted that the $\bar{D}$ values for the polymers prepared by the simultaneous copolymerization of styrene and isoprene monomers follow the same trend as the molecular-weight dependence of the D values for the

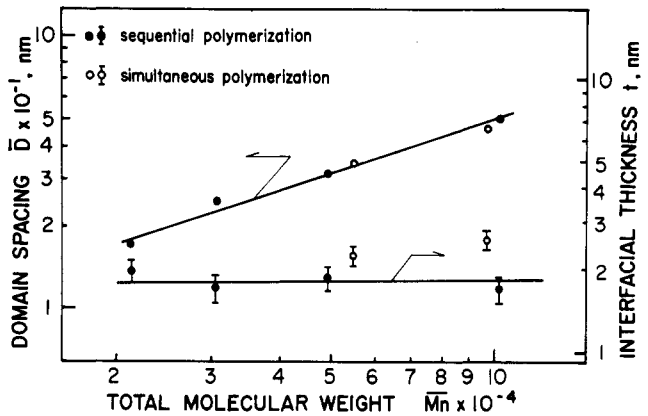

Figure 8. Measured average domain spacing $\bar{D}$ and interfacial thickness t as a function of total molecular weight for the block polymers prepared by the sequential polymerization (●) and by the simultaneous polymerization (○).

polymers prepared by the sequential polymerization of the two types of monomers. This is due to the fact that the reaction rate of styrene is much higher than that of isoprene in a THF medium so that the copolymerization may result in almost the same primary structure as the one prepared by the sequential polymerization.

The interfacial area occupied by a block polymer chain (S/N) was calculated by the relationship

$$S/N = 2(\bar{v}_A + \bar{v}_B)/\bar{D} \quad (7)$$

where $\bar{v}_K$ is the molecular volume of the K chain. This area increases with increasing molecular weight. Since $D \sim \bar{M}_n^{2/3}$ (thus $S/N \sim \bar{M}_n^{1/3}$)

$$S/N = 0.14\bar{M}_n^{1/3} \quad (\text{nm}^2) \quad (8)$$

It is noteworthy that the chemical junction points of the block polymers occupy a very minor portion of the interface. The majority of the interface is occupied by A and B segments which are not covalently bonded as at the chemical junction points but which rather have van der Waals interactions across the interface as in the polymer blends. This tendency increases with increasing molecular

weight, and at the limit of infinite molecular weight the block polymer interface should be identical with the interface of the polymer blend.

2. Interfacial Thickness. In the previous paper the scattered intensity at large-angle tail, $I(s)$, corrected for background scattering was shown to be given by[10]

$$I(s) = (\text{const})s^{-2} \exp(-4\pi^2\sigma^2 s^2) \quad (9)$$

where σ is the parameter characterizing the diffuseness of the boundary and the electron density variation of the system along the lamellar normal $\eta(z)$ is assumed to be given by a convolution product of a step function $g(z)$ and a Gaussian smoothing function $h(z)$ after Ruland[19]

$$\eta(z) = g(z) * h(z) \quad (10)$$

and

$$h(z) = (2\pi\sigma^2)^{-1/2} \exp(-z^2/2\sigma^2) \quad (11)$$

It should be noted that the scattering from the lamellar microdomain system with sharp boundaries varies according to s^{-2} rather than s^{-4}, due to the almost perfect orientation of the domains as shown earlier.[10]

Even when the lamellar domain system has some surface waviness or some size distribution in terms of T_A and T_B, eq 9 should still be valid if the wavelength of the wave is much larger than the interfacial thickness or if lamellae with sizes comparable to the interfacial thickness make a negligibly small contribution to the total scattering. These conditions are normally satisfied in our system as we discussed in section III. Generally the surface waviness and size distribution affect the proportional constant of eq 9 and push the Porod-law region toward higher scattering angles.

(a) Narrow-Interphase Approximation and Full Analysis. In the previous analysis[10] the interphase is assumed to be narrow so that one can approximate eq 9 by

$$I(s) = (\text{const})s^{-2}[1 - 4\pi^2\sigma^2 s^2 + O((\pi\sigma s)^4)] \quad (12)$$

Then σ can be evaluated from the slope and intercept at $s^{-2} = 0$ in the plot of $I(s)$ vs. s^{-2}. This assumption, designated as a narrow-interphase approximation, involves some errors due to truncation of the third and higher terms of the right-hand side of eq 12 and results in an interphase thinner than the actual interfacial thickness.[14] For example, for the L-6 specimen the ratio of the σ value estimated from the exact equation (9) to that estimated from eq 12 turns out to be 1.26.

A full analysis involves evaluation of σ from the slope of the plot $\ln I(s)s^2$ vs. s^2. Figure 9 shows a typical result for the L-6 specimen. From the slope, σ was evaluated to be 0.68 nm. Thus in this case the ratio of the second term to the third term of eq 12 is equal to about 0.73 at $s^2 = 8 \times 10^{-2}$ nm^{-2}, not negligibly small by any means.

(b) Definition of the Interfacial Thickness t Corresponding to the Linear Density Profile. In the previous analysis[10,14] t was related to σ by

$$t = 12^{1/2}\sigma \quad (13)$$

The scattered intensity from the pseudo-two-phase system having a trapezoidal electron density variation with thickness t at the boundary region is given by

$$I(s) = s^{-2} \sin^2(\pi st)/(\pi st)^2 = s^{-2}[1 - (\pi st)^2/3 + O((\pi st)^4)] \quad (14)$$

The relationship between σ and t was obtained by comparing eq 12 and 14 in the context of the narrow-interphase approximation.

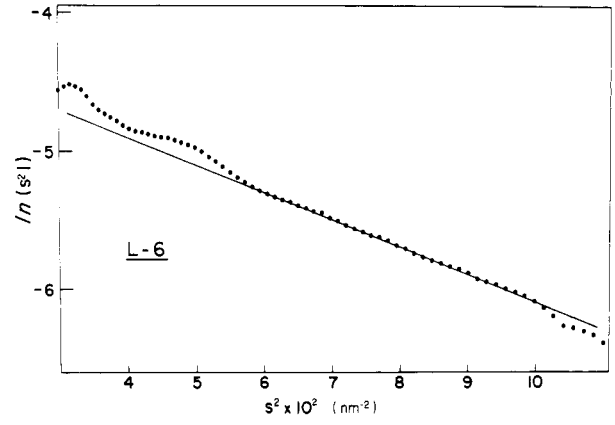

Figure 9. Full analysis of the interfacial thickness, ln $[s^2I(s)]$ vs. s^2.

Instead of using eq 13, we will define t in a more general way

$$t = 1/|\mathrm{d}\eta(z)/\mathrm{d}z|_{\eta=\Delta\rho_e/2} \quad (15)$$

where $\Delta\rho_e$ is the difference of electron densities between the polystyrene and polyisoprene lamellae. From eq 10 and 11, it follows that

$$\eta(z) = \pi^{-1/2}\Delta\rho_e \sum_{i=-N/2}^{N/2} \left\{\mathrm{Erf}\left(\frac{z + a - \bar{D}i}{2^{1/2}\sigma}\right) - \mathrm{Erf}\left(\frac{z - a - \bar{D}i}{2^{1/2}\sigma}\right)\right\} \quad (16)$$

where

$$\mathrm{Erf}\, x \equiv \int_0^x \exp(-t^2)\, \mathrm{d}t \quad (17)$$

and $a = T_{PS}/2$ (T_{PS} is the thickness of a polystyrene lamella), N is the number of pairs of the lamellae in the assembly, and $\bar{D}$ is the average lamellar spacing. In terms of the relative segment density $\tilde{\rho}_K$, t is defined by

$$t = 1/|\mathrm{d}\tilde{\rho}_K(z)/\mathrm{d}z|_{\tilde{\rho}_K=1/2} \quad (18)$$

From eq 15 and 16, t is given by, for small σ

$$t = (2\pi)^{1/2}\sigma \quad (18a)$$

(c) Results. The results of the interfacial thickness t corresponding to the linear density profile at the interface are summarized in Table II and plotted in Figure 8 as a function of total molecular weight. It should be noted that the interfacial thickness is not a strong function of molecular weight but rather almost independent of the molecular weight covered in this work. The thickness appears to decrease slightly with molecular weight if one carefully compares the results obtained only for the polymers prepared by the sequential polymerization (solid circles).

The thickness t for the polymer prepared by the simultaneous polymerization of the two monomers (open circles) turns out to be slightly larger than that for the polymer prepared by the sequential polymerization. Thus a slight perturbation of the primary structure involving a mixing of styrene and isoprene monomers near the chemical junction points enhances the mixing of the incompatible segments at the interface which results in the increased interfacial thickness.

One should note that the interfacial thickness t is a minimum estimation of the thickness for the interfacial region with a sigmoidal electron-density variation, i.e., almost half of the full thickness $\lambda \equiv |z_1 - z_2|$, where $\eta(z_1) \simeq 0$ and $\eta(z_2) \simeq \Delta\rho_e$ in eq 16. The relation between λ and

t is schematically shown in Figure 1. The volume fraction of the interfacial region f defined as $f = 2t/\bar{D}$ systematically decreases with increasing molecular weight as shown in Table II, which provides a key for understanding some physical properties of such heterophase systems.[20-25,30]

V. Comparison with Equilibrium Theories

Among the many theories which have been proposed to describe the equilibrium aspects of the domain morphology, the theories proposed by Meier[3-5] and Helfand and co-workers[6-8] seem to be the most elaborate and to be capable of describing the experimental evidence most quantitatively. In this section we compare the experimental results discussed in the foregoing sections with those predicted by the theories of Meier and Helfand.

1. Theories. In our previous paper[10] we compared the results for a particular block polymer (SI-L) with those predicted from theories based upon the assumption that the A and B chains were symmetric in terms of segment length, segment density, and degree of polymerization. The theories have been further generalized to account for the asymmetric effect[5,26] and we shall briefly discuss below the generalized theories, the results of which will be compared with the experimental results.

The change in Gibbs free energy accompanied by the phase transition from a uniform mixture of A and B segments to the microdomain structure, ΔG, was calculated by taking into account the three physical factors described in section I. According to Meier[5]

$$\frac{\Delta G}{NkT} = \frac{\chi_A}{4T_A}\left(\lambda + \frac{\pi^2 t_D^2}{6\lambda}\right) - \ln\left(\frac{2\lambda}{T_A + T_B}\right) + 1 - \ln\left\{\frac{8}{3}\frac{\lambda^2}{T_A' T_B'}\sum_{m,n=1}^{\infty} mn \sin\frac{m\pi}{2}\sin\frac{n\pi}{2} \times \exp\left[-\frac{\pi^2}{6}\left(\frac{m^2\sigma_A l_A^2}{(T_A')^2} + \frac{n^2\sigma_B l_B^2}{(T_B')^2}\right)\right]\right\} - \frac{\chi_A r(d_A/d_B)}{1 + r(d_A/d_B)} \quad (19)$$

where

$$T_K' = T_K + \lambda \qquad (K = A \text{ or } B) \quad (20)$$

and

$$T_B/T_A = \bar{v}_B/\bar{v}_A = r(d_A/d_B)$$
$$r = M_B/M_A \quad (21)$$

The quantities d_K and M_K are, respectively, the mass density and the molecular weight of K, T_K is the thickness of the K-lamellar domain, t_D is Debye's interaction range parameter, and σ_K and l_K are the number and length of the statistical segment of K. The quantity χ_A is the interaction parameter as defined by

$$\chi_A = \bar{v}_A\alpha$$
$$\alpha = (\delta_A - \delta_B)^2/kT \quad (22)$$

where δ_K is the solubility parameter of the K chain and k is Boltzmann's constant. N is the number of block polymer chains incorporated in the microphase separation.

The first term on the right-hand side of eq 19 is the term related to the interaction energy due to mixing of the incompatible A and B segments at the interfacial regions. The energy was calculated according to the Cahn–Hilliard formula[27] for a composition variation across the interphase $\phi_K(z)$ as given by

$$\phi_A(x) = \sin^2(\pi z/2\lambda) = 1 - \phi_B(x) \quad (23)$$

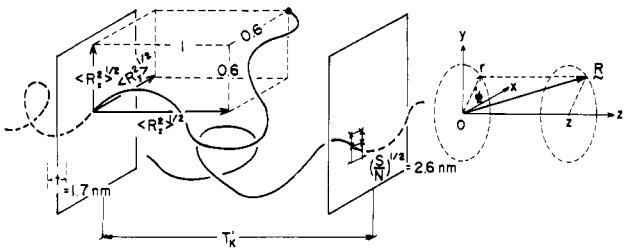

Figure 10. Root-mean-square end-to-end distance of a chain molecule in the domain space projected along the x, y, and z directions, $\langle R_x^2\rangle^{1/2}$, $\langle R_y^2\rangle^{1/2}$, and $\langle R_z^2\rangle^{1/2}$, respectively. The molecule is highly stretched along z, giving rise to $\langle R_z^2\rangle^{1/2}/\langle R_x^2\rangle^{1/2} = \langle R_z^2\rangle^{1/2}/\langle R_y^2\rangle^{1/2} \simeq 1.70$. The nearest-neighbor distance between the chemical junction points, which is approximately equal to $(S/N)^{1/2}$, is much smaller than the dimensions $\langle R_x^2\rangle^{1/2} = \langle R_y^2\rangle^{1/2}$, indicating a heavy overlap of neighboring molecules to produce a uniform filling of the space. $\langle R_z^2\rangle^{1/2}$ is also shown to be $T_K'/2$.

where λ is the parameter characterizing the thickness of the interphase. One can define as the interfacial thickness λ_I, corresponding to t in eq 15 or 18

$$\lambda_I = 1/|d\phi_K(z)/dz|_{\phi_K=1/2} = 0.637\lambda \quad (24)$$

The energy term decreases as $1/D$ with increasing domain size. The second and third terms are associated with the placement entropy loss, which increases ΔG in proportion to $\ln D$. The fourth term is associated with the entropy loss due to the constraint-volume effect and the requirement to maintain uniform segment density, which also increases ΔG with increasing D. The last term is the enthalpy of demixing. The combinatorial entropy contribution is trivial and ignored in this treatment.

Meier showed that the requirement of maintaining uniform density in the domain invokes a relation between the domain size and chain dimension.[3] For a lamellar domain this is given by[4]

$$T_K = 1.4\alpha_K\langle R_K^2\rangle_0^{1/2} \quad (25)$$

where α_K is the chain-expansion factor (along the lamellar normal) in the domain space caused by the constraint-volume and volume-filling effects but not by the excluded-volume effect. $\langle R_K^2\rangle_0$ is the unperturbed mean-square distance of K. From eq 19–25, one evaluates the equilibrium domain size D ($=T_A + T_B$) or the expansion factors α_A or α_B (α_A and α_B are mutually related by eq 21 and 25) and the interfacial thickness λ by minimizing ΔG with respect to D and λ. The process involves a numerical evaluation.

It should be noted that the theory does not account for the conformational entropy loss to maintain uniform density in the interphase of thickness λ.[39] This effect was assumed to be a trivial contribution to ΔG. In Helfand's theory,[6,7,28] this effect, however, was rigorously taken into account.

On the basis of random-flight chain statistics in the confined space as developed by Meier, one can calculate the probability $P(z, r, \phi)$ that one end of a chain is located at $\mathbf{R} = (z, r, \phi)$ when the other end (the chemical junction point) is located somewhere in the interphase under the constraint that all of the segments of the chain are confined between two walls separated by a distance T_K', as defined by eq 20 (see Figure 10)

$$P(z, r, \phi) \sim \exp\left(-\frac{3r^2}{2\sigma_K l_K^2}\right)\sum_{m=1}^{\infty}\sin\frac{m\pi z}{T_K'}\exp\left[-\frac{m^2\pi^2\sigma_K l_K^2}{6(T_K')^2}\right] \quad (26)$$

The uniform volume-filling requirement again invokes eq

25. From eq 26, the mean-square end-to-end distance projected onto the x, y, and z axes ($\langle R_x^2\rangle$, $\langle R_y^2\rangle$, and $\langle R_z^2\rangle$, respectively) can be calculated

$$\langle R_z^2\rangle = \int_0^{2\pi} d\phi \int_0^{\infty} r\, dr \int_0^{T_K'} dz\, z^2 P(z, r, \phi) \Big/ \int_0^{2\pi} d\phi \int_0^{\infty} r\, dr \int_0^{T_K'} dz\, P(z, r, \phi)$$

$$= (T_K')^2 \left\{ \sum_{m=1}^{\infty} \frac{1}{m^2}[(-1)^{m+1} m^2\pi^2 + 2(-1)^m - 2] \times \exp(-m^2\pi^2/12\alpha_K^2) \right\} \Big/ \left\{ 2\pi^2 \sum_{\substack{m=1 \\ (\text{odd})}}^{\infty} \exp(-m^2\pi^2/12\alpha_K^2) \right\} \simeq (T_K')^2/4 \quad (27)$$

Similarly

$$\langle R_x^2\rangle = \langle R_y^2\rangle = \tfrac{1}{2}\langle r^2\rangle = \tfrac{1}{3}\sigma_K l_K^2 \quad (28)$$

These results will be discussed in section V-3 in relation to the molecular packing in the domain space.

Helfand has also developed theories of microdomain structure on the basis of random-flight chain statistics in the confined space but in a more elaborate fashion than Meier. Here we shall contrast the experimental results with those predicted from the theories based on the narrow-interphase approximation,[7] appropriate when the interfacial thickness is small compared with the domain size. In this case the free energy change of the microdomain formation is given by[7]

$$\frac{\Delta G}{NkT} = \frac{2\gamma}{kT}\left(\frac{Z_A}{\rho_{0A}} + \frac{Z_B}{\rho_{0B}}\right)\frac{1}{D} - \ln\frac{2a_J}{D} + 0.141\frac{(Z_A^{1/2}/b_A\rho_{0A})^{2.5} + (Z_B^{1/2}/b_B\rho_{0B})^{2.5}}{[(Z_A/\rho_{0A}) + (Z_B/\rho_{0B})]^{2.5}} D^{2.5} - \frac{\alpha(Z_A/\rho_{0A})(Z_B/\rho_{0B})}{(Z_A/\rho_{0A}) + (Z_B/\rho_{0B})} \quad (29)$$

where γ is the interfacial tension and is given by

$$\gamma = kT\alpha^{1/2}\left[\frac{\beta_A + \beta_B}{2} + \frac{1}{6}\frac{(\beta_A - \beta_B)^2}{\beta_A + \beta_B}\right] \quad (30)$$

a_J is a measure of the freedom of motion of a block copolymer joint which is closely related to a characteristic thickness a_I of an interphase

$$a_I \equiv (dz/d\tilde{p}_A)_{\tilde{p}_A=1/2} = 2\left[\frac{\beta_A^2 + \beta_B^2}{2\alpha}\right]^{1/2} \quad (31)$$

$$\beta_K = \rho_{0K} b_K^2/6$$

$$b_K^2 = \langle R_K^2\rangle_0/Z_K \quad (32)$$

The quantity b_K is Kuhn's statistical segment length and Z_K is the degree of polymerization of the K-block chain. The parameter α is defined in eq 22. The interfacial thickness a_I is the thickness corresponding to t in eq 15 and λ_1 in eq 24. The equilibrium value of D is given by minimizing ΔG with respect to D.

The first term on the right-hand side of eq 29 is associated with the interfacial free energy which is composed of the interaction energy of mixing the A and B segments and the loss of conformational entropy to maintain a uniform density in the interphase. The second term is loss of the placement entropy and the third term is associated with the loss of the conformational entropy due to the constraint volume and chain perturbations in the domains. Finally the last term is the enthalpy of demixing.

Equations 30 and 31 were obtained by neglecting the nonlocality of the energetic interactions (thus corresponding to the case of $t_D = 0$ in eq 19). This effect of nonlocality of interactions is taken into account in the works of Helfand and Tagami[28] for symmetric polymers and Helfand and Sapse[26] (HS) for asymmetric polymers. In the latter case γ in eq 30 should be replaced by eq 6.7 of HS and a_I in eq 31 should be calculated from eq 6.5 of HS, the results of which turn out to be given by the explicit formula

$$a_{I,n} = 2\left[\frac{\beta_A^2 + \beta_B^2}{2\alpha} + \frac{1}{6}\sigma_I^2\right]^{1/2} \quad (33)$$

where σ_I is the interaction range parameter for monomer units (cf. t_D being defined as the interaction range parameter for the segmental units).

2. Parameters Required for the Comparisons. From the preceding section, it is obvious that one needs to know the statistical segment lengths (b_{PS} and b_{PI}), the number density of monomeric units (ρ_{0PS} and ρ_{0PI}) for polystyrene and polyisoprene, respectively, and the interaction parameter α if a comparison between the experimental results and theoretical predictions is to be made.

The statistical segment length used is the value reported by Ballard, Wignall, and Schelten from neutron scattering experiments for bulk polystyrene[29]

$$b_{PS} = 0.68 \text{ nm}$$

or

$$[\langle R_{PS}^2\rangle_0/\bar{M}_{PS}]^{1/2} = 0.067 \text{ nm}$$

For polyisoprene having a high vinyl content, we measured[12]

$$b_{PI} = 0.59 \text{ nm}$$

or

$$[\langle R_{PI}^2\rangle_0/\bar{M}_{PI}]^{1/2} = 0.072 \text{ nm}$$

The densities of the pure polymers were measured by the density gradient tube method

$$\rho_{0PS} = 1.01 \times 10^4 \text{ mol/m}^3$$

$$\rho_{0PI} = 1.36 \times 10^4 \text{ mol/m}^3$$

As for the interaction parameter α, we adopted a room-temperature value obtained by the formula of Rounds and McIntyre as cited by Helfand[7]

$$\alpha = (\delta_A - \delta_B)^2/kT = -900 + 7.5 \times 10^5/T \text{ mol/m}^3 \quad (34)$$

It should be noted that this result was obtained for polystyrene and *cis*-1,4-polyisoprene and is not strictly applicable to the interaction with polyisoprene having a high vinyl content. This is a weak point in our analysis. The value of t_D is set to be 0.8 nm as in Meier's works.[5,40]

3. Discussion. (a) Molecular Packing and Domain Size. Figure 10 represents a schematic diagram showing the packing of the chain molecules in the domain space. For the polystyrene domain of the L-6 specimen, for example, it turns out from eq 27 and 28

$$\langle R_x^2\rangle^{1/2} = \langle R_y^2\rangle^{1/2} = 9.6 \text{ nm}$$

$$\langle R_z^2\rangle^{1/2} \simeq T_{PS}'/2 = 16.4 \text{ nm}$$

Thus the ratio $\langle R_z^2\rangle^{1/2}/\langle R_x^2\rangle^{1/2} = 1.70$, indicating that the

Table III
Comparison of Measured and Predicted Domain Properties of the Lamellar Domain System of Styrene-Isoprene Diblock Polymers

specimen code	$10^{-3}\bar{M}_n$	wt % PS	domain spacing, nm			interfacial thickness, nm		
				calcd			calcd	
			exptl	Meier	Helfand	exptl (t)	Meier (λ_I)	Helfand (a_I)
L-1	21	53	17.2	19.8	19.3	2.0 ± 0.2	3.4	1.4
L-2	31	40	24.3	26.2	25.2	1.7 ± 0.2	3.4	1.4
L-3	49	45	31.9	36.0	34.7	1.9 ± 0.2	3.3	1.4
L-4[a]	55	46	34.0	38.7	37.4	2.3 ± 0.2	3.2	1.4
L-5[a]	97	51	46.3	55.5	54.9	2.6 ± 0.2	2.8	1.4
L-6	102	61	50.3	56.9	56.2	1.7 ± 0.2	2.8	1.4

[a] Polymerized by a slightly different procedure. The calculated values correspond to those for pure diblock copolymers.

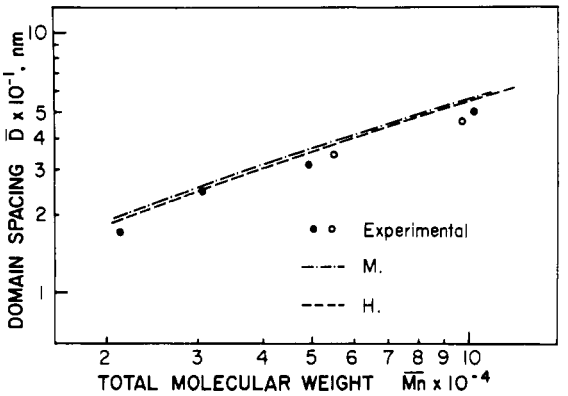

Figure 11. Measured (circles) and predicted domain spacing $\bar{D}$ as a function of total molecular weight of the block polymers. M and H stand for the results calculated from Meier's and Helfand's theories.

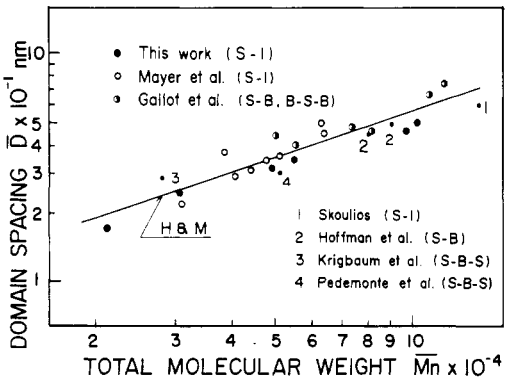

Figure 12. Comparison between measured and calculated average domain spacings as a function of total molecular weight of block polymers. The calculated $\bar{D}$ was obtained from the theories of Helfand and Meier for diblock polymers having equal molecular weights with parameters as in section V-2 in the text. A-B-A polymers were treated as the diblock polymers of A-(1/2)B. The symbols S and B stand for polystyrene and polybutadiene, respectively. The data indicated by large filled circles, open circles, and half-filled circles were obtained in this work, the work by Mayer et al.,[31,32] and the work by Gallot et al.,[32-34] respectively. The small solid circles numbered from 1 to 4 were taken from the works of Skoulios,[35] Hoffmann et al.,[36] Krigbaum et al.,[37] and Pedemonte et al.,[38] respectively.

chain is expected to be expanded along the lamellar normal. The nearest-neighbor distance between the two chemical junction points is approximated by $(S/N)^{1/2}$ = 2.6 nm, roughly equal to the interfacial thickness, 1.7 nm. This distance S/N is much smaller than $\langle R_x^2 \rangle^{1/2}$ and $\langle R_y^2 \rangle^{1/2}$, indicating that neighboring molecules overlap heavily to result in a uniform filling of the space.

Table III summarizes a comparison of the measured and calculated domain spacings and interfacial thicknesses (the latter quantity is discussed later). The calculated values were obtained for the parameters as described in section V-2. The interaction range parameter was set as follows: $\sigma_I = 0$ (Helfand's equation) and $t_D = 0.8$ nm (Meier's equation). The results for the domain spacing are plotted in Figure 11. The spacings predicted from Meier's theory (M) and Helfand's theory (H) agree with each other and also with our experimental results, marked by the solid (for sequentially polymerized materials) and open circles (for simultaneously polymerized materials), in terms of both absolute values and molecular-weight dependencies. This may indicate that the size of the lamellar microdomain is predictable by the equilibrium theories and that the global conformation of the chain molecules in the domain space can essentially be described by the random-flight chain statistics.

This is further confirmed by the results shown in Figure 12 in which we have plotted the lamellar spacings as a function of total molecular weight for the diblock polymers styrene–isoprene (S–I) and styrene–butadiene (S–B) and the triblock polymers butadiene–styrene–butadiene (B–S–B) and styrene–butadiene–styrene (S–B–S) obtained by Mayer et al.[31,32] (large open circles), Gallot et al.[32-34] (large half-filled circles), Skoulios[35] (small solid circle marked by 1), Hoffmann et al.[36] (small solid circles marked by 2), Krigbaum et al.[37] (small solid circles marked by 3), and Pedemonte et al.[38] (small solid circle marked by 4). The solid line is the result predicted by the Helfand and Meier theories for diblock polymers having equal molecular weights for polystyrene and polyisoprene (parameters as described in section V-2). It should be noted that the morphology of the triblock polymers S–B–S and B–S–B is approximately equal to that of the diblock polymers S–(1/2)B and B–(1/2)S, respectively. We used this relationship in the plot of Figure 12.

The spacings for the block polymers having a high content of *cis*-1,4-polyisoprene are slightly larger (about 7%) than those for the polymers having a high vinyl content since the statistical segment length of the former is larger than that of the latter. Figure 12 confirms the conclusion that the lamellar domain system is predictable by the equilibrium theories and, therefore, by molecular and thermodynamic parameters such as Z_K, ρ_{0K}, b_K, and α, although there is some scattering in the data points primarily owing to the difference in the chemical composition for each polymer.

(b) Interfacial Thickness t. The measured and calculated interfacial thicknesses are summarized in Table III. The interfacial thicknesses were calculated for the same set of parameters as in the calculation of the domain spacing.

The interfacial thickness a_I calculated from Helfand's theory is constant, 1.4 nm, independent of molecular weight, which is a consequence of invoking the narrow-

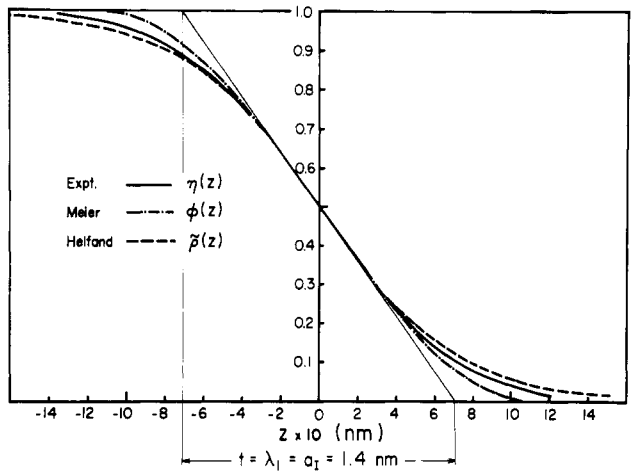

Figure 13. Comparison of the electron density profiles at the interphase assumed in the SAXS analyses, $\eta(z)$, and in Meier's theory, $\phi(z)$, and calculated by Helfand's theory, $\tilde{p}(z)$, for a given interfacial thickness $t = \lambda_I = a_I = 1.4$ nm.

interphase approximation and of a_I being calculated for an infinitely large molecular weight limit. On the other hand, the interfacial thickness λ_I calculated from Meier's theory depends on molecular weight, decreasing with increasing molecular weight (according to $M^{-1/3}$) to an asymptotic value of $t_D = 0.8$ nm. Thus in the limit of infinite molecular weight, Helfand's interfacial thickness is much larger than Meier's interfacial thickness. This excess interfacial thickness may be stabilized by the nonlocal aspects of conformational entropy[39] and by the loss of conformational entropy required to maintain uniform density in the interphase, which Meier's theory ignores.

Although there are some discrepancies between the measured and calculated interfacial thicknesses, we may conclude that the experimental results agree with the calculated results. The discrepancies are still within the errors involved in estimating the interaction parameter α at the present stage. It is crucial to obtain an accurate value of α in order to distinguish the theories.

Figure 13 shows a comparison of the relative segment density profiles of the function $\eta(z)$ (eq 10) assumed for the SAXS analysis, $\phi_K(z)$ (eq 23) assumed in Meier's calculation, and $\tilde{p}_K(z)$ calculated from Helfand's theory for a given interfacial thickness $t = \lambda_I = a_I = 1.4$ nm. These three functions are shown to be quite similar.[42] If one used the function $\tilde{p}(z)$ ($\phi(z)$) used by Helfand (Meier) instead of using $\eta(z)$, one would obviously obtain an interfacial thickness slightly greater (smaller) than the estimated value of t. Thus the discrepancies among the three values t, λ_I, and a_I in Table III would become slightly but not significantly smaller.

(c) Effect of Asymmetry. In our previous paper[10] we compared the experimental results on a particular block polymer with those predicted by the theories for the "symmetric" block polymers. It is worthwhile to study here the errors involved in the assumption of the symmetry by comparing the results with those obtained for general "asymmetric" block polymers. We have illustrated this effect in Table IV for a particular S–I diblock polymer having equal block molecular weights of 5×10^4.

In the hypothetical symmetric block polymers, the segment densities of polystyrene and polyisoprene are assumed to have $\rho_0 = (\rho_{0S}\rho_{0I})^{1/2} = 11.7 \times 10^3$ mol/m^3. Polystyrene and polyisoprene are assumed to have hypothetically equal statistical segment lengths, $b = 0.63$ nm ($\rho_0 b^2 = [\rho_{0I} b_I^2 + \rho_{0S} b_S^2]/2$) and degrees of polymerization, $Z = 593.6$ ($\alpha Z/\rho_0 = [Z_S/\rho_{0S} + Z_I/\rho_{0I}]/2$). It turns out from

Table IV[a]
Effects of the Nonlocality of Energetic Interactions and of the Asymmetry of Block Chains on the Estimated Values of the Domain Spacing $\bar{D}$ and the Interfacial Thickness t

interaction range parameter, nm	asymmetry, nm		symmetry, nm		
	$\bar{D}$	a_I or λ_I	$\bar{D}$	a_I or λ_I	remarks
$\sigma_I = 0.5$	56.6	1.43	56.2	1.43	H, nonlocal
$\sigma_I = 0$	56.0	1.38	55.7	1.37	H, local
$t_D = 0.8$	56.5	2.82	57.3	2.55	M, nonlocal
$t_D = 0$	55.4	2.67	55.9	2.35	M, local

[a] Calculated for an S-I diblock having equal block molecular weights (5×10^4). The symbols H and M stand for the values obtained from Helfand's and Meier's theory.

Table IV that the errors involved by assuming symmetry are actually small.

(d) Effect of Nonlocal Energetic Interaction. In Table III, the values predicted from Helfand's theory are based on localized interaction (i.e., $\sigma_I = 0$), while those from Meier's theory are based on nonlocalized interaction ($t_D = 0.8$ nm). It is therefore worthwhile to study the effect of nonlocalized interaction on the estimated domain spacing $\bar{D}$ and the interfacial thickness a_I or λ_I. This effect is summarized in Table IV. It is shown that the spacing and the interfacial thickness tend to increase slightly with increasing interaction range parameter σ_I or t_D. The amount of increase, however, is negligibly small.

Acknowledgment. This work was supported by a Grant-in-Aid for Scientific Research from the Ministry of Education, Japan (243021).

References and Notes

(1) G. E. Molau, "Block Polymers", S. L. Aggarwal, Ed., Plenum Press, New York, 1970, p 79.
(2) T. Inoue, T. Soen, T. Hashimoto, and H. Kawai, *J. Polym. Sci., Part A-2*, **7**, 1283 (1969).
(3) D. J. Meier, *J. Polym. Sci., Part C*, **26**, 81 (1969).
(4) D. J. Meier in "Block and Graft Copolymers", J. J. Burke and V. Weiss, Eds., Syracuse University Press, Syracuse, N.Y., 1973, p 105.
(5) D. J. Meier, *Prepr. Polym. Colloq., Soc. Polym. Sci., Jpn.*, 83 (1977).
(6) E. Helfand, *Macromolecules*, **8**, 552 (1975).
(7) E. Helfand and Z. R. Wasserman, *Macromolecules*, **9**, 879 (1976).
(8) E. Helfand and Z. R. Wasserman, *Macromolecules*, **11**, 960 (1978).
(9) T. Hashimoto, K. Nagatoshi, A. Todo, H. Hasegawa, and H. Kawai, *Macromolecules*, **7**, 364 (1974).
(10) T. Hashimoto, A. Todo, H. Itoi, and H. Kawai, *Macromolecules*, **10**, 377 (1977).
(11) P. Debye, *J. Chem. Phys.*, **31**, 680 (1959).
(12) T. Hashimoto, N. Nakamura, M. Shibayama, A. Izumi, and H. Kawai, *J. Macromol. Sci.—Phys.*, **B17** (3), 389 (1980).
(13) J. Bandrup and E. H. Immergut, Eds., "Polymer Handbook", Wiley, New York, 1975, Chapter IV-4.
(14) A. Todo, T. Hashimoto, and H. Kawai, *J. Appl. Crystallogr.*, 11, 558 (1978).
(15) A. Keller, E. Pedemonte, and F. M. Willmouth, *Kolloid Z.*, **238**, 385 (1970).
(16) M. J. Folkes and A. Keller, "Block and Graft Copolymers", J. J. Burke and V. Weiss, Eds., Syracuse University Press, Syracuse, N.Y., 1973, p 87.
(17) (a) J. Rathie and W. Ruland, *Colloid Polym. Sci.*, **254**, 358 (1976). (b) R. Hosemann and S. N. Bagchi, "Direct Analysis of Diffraction by Matter", North-Holland, Amsterdam, 1962.
(18) C. G. Vonk, *J. Appl. Crystallogr.*, **6**, 81 (1973).
(19) W. Ruland, *J. Appl. Crystallogr.*, **4**, 70 (1971).
(20) M. Shen and D. H. Kaelble, *J. Polym. Sci., Part B*, **8**, 149 (1970).
(21) D. G. Fesko and N. W. Tschoegl, *Int. J. Polym. Mater.*, **3**, 51 (1974).
(22) T. Soen, M. Shimomura, T. Uchida, and H. Kawai, *Colloid Polym. Sci.*, **252**, 933 (1974).

(23) G. Kraus and K. W. Rollmann, *J. Polym. Sci., Polym. Phys. Ed.*, 14, 1133 (1976).
(24) A. Todo, H. Uno, K. Miyoshi, T. Hashimoto, and H. Kawai, *Polym. Eng. Sci.*, 17, 587 (1977).
(25) H. Odani, K. Taira, N. Nemoto, and M. Kurata, *Polym. Eng. Sci.*, 17, 527 (1977).
(26) E. Helfand and A. M. Sapse, *J. Chem. Phys.*, 62, 1327 (1975).
(27) J. W. Cahn and J. E. Hilliard, *J. Chem. Phys.*, 28, 258 (1958).
(28) E. Helfand and Y. Tagami, *J. Chem. Phys.*, 62, 1327 (1975).
(29) D. G. H. Ballard, G. D. Wignall, and J. Schelten, *Eur. Polym. J.*, 9, 965 (1973).
(30) T. Hashimoto, M. Fujimura, K. Saijo, H. Kawai, J. Diamont, and M. Shen, *Adv. Chem. Ser.*, No. 176, 257 (1979).
(31) R. Mayer, *Polymer*, 15, 137 (1974).
(32) A. Douy, R. Mayer, J. Rossi, and B. Gallot, *Mol. Cryst. Liq. Cryst.*, 7, 103 (1969).
(33) C. Sadron and B. Gallot, *Makromol. Chem.*, 164, 301 (1973).
(34) A. Douy and B. Gallot, *Makromol. Chem.*, 156, 81 (1972).
(35) A. E. Skoulios, "Block and Graft Copolymers", J. J. Burke and V. Weiss, Eds., Syracuse University Press, Syracuse, N.Y., 1963.
(36) M. Hoffmann, G. Kämpf, H. Krömer, and G. Pampus, *Adv. Chem. Ser.*, No. 99, 351 (1971).
(37) W. R. Krigbaum, S. Yazgan, and W. R. Tolbert, *J. Polym. Sci., Polym. Phys. Ed.*, 11, 511 (1973).
(38) E. Pedemonte and G. C. Alfonso, *Macromolecules*, 8, 85 (1975).
(39) The first term on the right-hand side of eq 19 in Meier's theory[40] (derived on the basis of the Cahn–Hilliard formula with the assumed density distributions on $\phi_K(x)$ in eq 23) neglects the nonlocal aspects of the conformational entropy[26,28] which arises from the chemical bonding of segmental units, i.e., the requirement of a segmental unit at r having another segment a vector of distance b away. For a symmetric block an explicit formula for λ is obtained by minimizing ΔG with respect to λ[10]

$$\lambda = \frac{6T_A}{\chi_A Z_A} + \left[\left(\frac{6T_A}{\chi_A Z_A}\right)^2 + \frac{1}{6}\pi^2 t_D^2\right]^{1/2}$$

λ approaches λ_∞ with increasing molecular weight

$$\lambda \to \lambda_\infty = (\pi/6^{1/2})t_D$$

or

$$\lambda_I \to \lambda_{I,\infty} = 0.817 t_D$$

The corresponding interfacial thickness a_I predicted from Helfand's theory is given, from eq 33, by

$$a_I = (2/6^{1/2})[(b^2/\chi) + \sigma_I^2]^{1/2}$$

and gives a thicker interphase than λ_I. a_I approaches $a_{I,0}$ for small values of b

$$a_I \to a_{I,0} = (2/6^{1/2})\sigma_I = 0.816\sigma_I$$

Thus in the limit of $b = 0$, the two results become identical.
(40) D. J. Meier, *Polym. Prepr., Am. Chem. Soc., Div. Polym. Chem.*, 15, 171 (1974).
(41) The condition $g \gtrsim 0.035$ is necessary; otherwise a 10th-order peak should be resoluble.
(42) This does not mean that all three values t, λ_I, and a_I are in agreement. A comparison of the absolute values is shown in Table III.

Ionic Strength Dependence of the Average Dimension of Low Molecular Weight DNA

M. Mandel* and J. Schouten

Department of Physical Chemistry, Gorlaeus Laboratories, University of Leiden, 2300 RA Leiden, The Netherlands. *Received February 12, 1980*

ABSTRACT: Light scattering measurements are reported for sonicated calf-thymus DNA of known contour length (l) distribution in buffer solutions at five different ionic strengths ($5 \times 10^{-3} \leq I \leq 2 \times 10^{-1}$ M). The change with ionic strength of the root-mean-square radius of gyration as determined from these measurements for the relatively short macromolecules ($M_w = 3 \times 10^5$ g mol^{-1}, $l_w = 167$ nm) of high intrinsic rigidity is compared to theoretical predictions based on a wormlike chain with an electrostatic part of the persistence length (Odijk). The agreement is satisfactory if partial charge compensation (condensation) is taken into account.

One of the central problems in the physical chemistry of polyelectrolyte solutions is the influence of the charge interactions on the average dimension of the polyions. Recently a new theoretical approach to this problem was proposed independently by Odijk from this laboratory[1,2] and by Skolnick and Fixman in the U.S.A.[3] Considering a polyion as a wormlike chain with an intrinsic stiffness, characterized by a "bare" persistence length L_p, they calculated the increase in the stiffness due to the charges on the chain interacting through a Debye–Hückel potential with a screening length κ^{-1} depending on the ionic strength I of the solution. The expression for the additional "electrostatic" persistence length L_e is assumed to be valid under the condition that $L_p + L_e \gg \kappa^{-1}$[3,4] and depends linearly on κ^{-2}. The total persistence length $L_t = L_p + L_e$ may be used to evaluate the average dimension of a polyion, e.g., its root-mean-square radius of gyration. As this quantity at infinite dilution may be obtained through light scattering measurements, these theoretical predictions can, in principle, be checked. A particularly suitable system should be DNA which even at considerably high ionic strength ($I = 0.2$ M) seems to behave in a way consistent with a description as a wormlike chain because of its high intrinsic stiffness.

We present here some experimental results obtained with DNA of low molecular weight (for which excluded-volume effects should be negligible) at five different ionic strengths. We show that the increase in the root-mean-square radius of gyration $\langle S^2 \rangle^{1/2}$ over the range $I = 0.2$ M to $I = 0.005$ M is rather small (<5%) and in fair agreement with the theoretical predictions, at least if charge compensation (condensation) is taken into account. However, as the DNA system used was heterodisperse, this conclusion remains preliminary.

Materials and Methods

All chemicals were of analytical reagent grade. Water was deionized by a mixed-bed ion exchanger (Amberlite HB-1). The Na salt of calf-thymus DNA (Worthington Biochemical Co.) of low protein content (<0.9%) was sonicated for 9 min at a concentration of approximately 0.3 mg cm^{-3} in 0.2 NaCl/0.002 M EDTA/0.002 M Na_2HPO_4 buffer, saturated with chloroform, and at a frequency of 21 kHz. The sonicated DNA has been fully characterized as described elsewhere (as DNA II).[5] It was heterodisperse with number-, weight-, and z-average contour lengths

0024-9297/80/2213-1247$01.00/0